Giant Pockels effect in ZnO-F films deposited on bare glasses

2002 J. Phys.: Condens. Matter 14 5407

(http://iopscience.iop.org/0953-8984/14/21/315)

INSTITUTE OF PHYSICS PUBLISHING JOURNAL OF PHYSICS: CONDENSED MATTER

J. Phys.: Condens. Matter **14** (2002) 5407–5417 PII: S0953-8984(02)34640-X

Giant Pockels effect in ZnO–F films deposited on bare glasses

I V Kityk[1], **J Ebothe**[2], **A El Hichou**[2], **M Addou**[3], **A Bougrine**[3] **and B Sahraoui**[4]

[1] Institute of Physics WSP, Al. Armii Krajowej 13/15, Czestochowa, Poland
[2] Université de Reims, UFR Sciences, UTAP–LMET, UPRES EA no 2061, 21 rue Clement Ader, 51865 Reims, Cedex 03, France
[3] LOPCM, Université Ibn Tofail, Faculte des Sciences, BP 133, Kenitra, Maroc
[4] Laboratoire POMA, Université d'Angers, UMR CNRS 6106, bld Lavouisier 2, Cedex 02, Angers, France

E-mail: i.kityk@wsp.czest.pl

Received 14 February 2002, in final form 22 April 2002
Published 16 May 2002
Online at stacks.iop.org/JPhysCM/14/5407

Abstract

A giant linear electro-optics (Pockels) effect (up to 17 pm V^{-1}) (for wavelength about 435 nm) in ZnO crystalline films doped with fluorine and deposited on bare glass has been found. For description of the observed phenomenon, a complex approach including self-consistent band structure calculations together with an appropriate molecular dynamics simulation of the interface structure was applied. Experimental ellipsometric and refractive index measurements confirm an efficiency of the mentioned approach for description of the observed interface (between the film and glass) processes. The origin of the observed effect is caused by substantial non-centrosymmetric charge density distribution between the ZnO wurtzite-like crystalline films and the bare glass substrate, as well as by additional charge density polarization caused by fluorine atoms.

(Some figures in this article are in colour only in the electronic version)

1. Introduction

The wurtzite-like ZnO single crystals possess hexagonal symmetry (space group C_{6v}^4), and due to the lack of a centre of symmetry they may possess properties described by third-order polar tensors. They have a good transparency in the visible region and have energy gaps equal to about 3.2–3.3 eV. Oriented wurtzite-like polycrystalline ZnO films were produced by deposition on different (Si, GaAs, GaN etc) substrates etc using several techniques [1, 2]. The morphology of the film surfaces was sensitive to doping by different atoms, particularly by Al [3], fluorine [4] etc. Such films are promising for use in different devices, for example the mentioned films possess large green luminescence at $\lambda = 540$ nm [5]. In [6] the lack

of a centre of symmetry, together with a large electromechanical coupling, results in a large piezoelectric effect, which is just being applied in industry.

Unfortunately, in most of the investigations the role of the thin interface layers between the films and substrates is neglected. However, the thin interface layers (possessing thickness up to several nanometres) may play a key role in the optical and non-linear optical phenomena requiring large values of inter-band transition dipole moments. Usually the interfaces possess relatively large dipole moments due to large gradients of the energy gaps and jumps of electrostatic potentials on the corresponding inter-phase borders.

From general phenomenological consideration one can expect that the mentioned materials should also possess good second-order non-linear optical properties. For example in [7] photoinduced optical second-harmonic generation has just been reported. Particular interest may be presented by the linear electro-optics effect (LEE), or the Pockels effect described by the third-order polar tensor. The applications of the film–glass interfaces, as well as appropriate doping, are promising ways for enhancement of the LEE. To perform a search for appropriate doping we have applied a complex approach including theoretical band structure (BS) and molecular dynamics (MD) simulations. In this paper we simulate linear and non-linear optical properties of the mentioned interfaces using these approaches.

The technique of specimen preparation, their features and measurement set-up are presented in section 2. In section 3 we present results of the MD simulations of interfaces. BS results are presented in section 4. Results of the imaginary part of dielectric susceptibilities (obtained experimentally and simulated theoretically) together with the evaluated LEE coefficients are given in section 5. We show that the origin of the experimentally observed Pockels effect is caused both by ZnO–glass interfaces as well as by fluorine doping.

2. Experimental methods

2.1. Specimen preparation and their features

The investigated zinc oxide thin films were obtained from a spraying process whose related set-up is fully described elsewhere [19]. This one is equipped with a nozzle kept above the support of the film substrate in such a way that the flow of the deposition bath is oriented perpendicularly to the substrate plane. For pure ZnO specimens, this bath consists of an aqueous solution prepared from a Fluka $ZnCl_2$ product of 0.05 M (Zn^{2+}) concentration whose pH = 3 value is maintained by a small addition of hydrochloric acid to prevent the formation of $Zn(OH)_2$. The fluorine-doped specimens are obtained from the same (Zn^{2+}) solution wherein is added (F^+) species prepared from NH_4F Fluka product to achieve the desired final atomic content of the material, ZnO:F(6%), determined from energy-disperse x-ray spectrometry. In both cases, the bath is activated by air carrier gas in order to produce a precise flow rate value, f, the substrate–nozzle distance $d = 44.5$ cm being kept constant. The film formation occurs on deposition substrates made of glass soda limes whose temperature is fixed at $T_s = 723$ K. This relatively high temperature leads to formation of pure materials in polycrystalline form. The deposition time is adjusted to the f value used in order to produce the same 1 μm thick film. This thickness has been confirmed from the sample cross-sectional images obtained by scanning electron microscopy. The material structure analysis, studied by x-ray diffraction (XRD) using Kα Cu radiation $\lambda = 0.1542$ nm, reveals that the fluorine doping has absolutely no influence on the morphology of the layer. Hexagonal structure is always obtained, the films bearing a (002) preferred growth orientation normal to the substrate plane. The x-ray diffractometry measurements performed using a DRON-05 x-ray diffractometer have given the film's crystalline parameters as presented in table 1. Moreover the parameters of the

Table 1. Typical crystalline parameters a and c for the ZnO films possessing different thicknesses and contents.

Type of film (μm)	a (nm)	c (nm)	Concentration of F (wt%)
ZnO (1.2)	2.966(7)	5.381(4)	0
ZnO (2.6 μm)	2.962(4)	5.375(4)	0
ZnO (0.9 μm)	2.969(4)	5.389(4)	0
ZnO–F (2.6 μm)	2.972(4)	5.384(3)	1
ZnO–F (2.6 μm)	2.970(8)	5.386(2)	1.5

unit cells (determined by x-ray) for the particular crystallites are independent of technology. Varying the f value, we were able to control the morphology of the layer. This aspect is characterized by atomic force microscopy (AFM) using a stand-alone SMENA set-up that operates in a constant-force contact mode. Its cantilever was made of a commercial Si_3N_4 tip of $\approx$50 nm apex radius whose spring coefficient is 0.06 N m^{-1}. This study is performed in ambient atmosphere, the AFM images being digitized into 400 $\times$ 400 pixels with a scanning frequency of about 1 Hz. In figures 1(a) and (b) one can see that depending on the f value the mean grain size of the films $\langle d_s \rangle$ is changed in the desirable directions. In this case the interface between the layer and the glass substrate could play a crucial role for the optical properties.

The data presented in table 1 unambiguously show that the crystalline structure of the produced films is only slightly dependent on the film thickness and the presence of fluorine. Reproducibility of the films may be achieved with controlled crystalline parameters but also with the same morphological structure. Thus the main effects may be expected only on the interfaces, that may be manifested using optical methods.

2.2. Measurement technique

The measurements of the LEE coefficients were made using the traditional Senarmone method [8]. The principal measurement set-up is presented in figure 2.

The monochromatic light (with given wavelength λ) from the grating spectrophotometer SP was polarized by polarizer P. The wavelengths were varied within the spectral range 380–900 nm. The electrodes (E) allow us to apply the electrostatic field in a direction perpendicular to the light propagation (these directions we indicate by 2 and 3, respectively). Rotating the electro-optically operated phase-plate ($\lambda/4$) we also varied phase angles ϕ to determine values of birefringence Δn for every external voltage. From the obtained ϕ-dependent light intensities for each wavelength we have evaluated the birefringence:

$$\Delta n = \lambda\phi/d, \tag{1}$$

where λ is the monochromatic wavelength; d is the film thickness determined by the interferometric method. The precision of the birefringence evaluation was about 5 $\times$ 10^{-5}. The LEE components were evaluated with accuracy up to 0.005 pm V^{-1}. The grating monochromator's spectral resolution was equal to about 0.4 nm mm^{-1}. To evaluate the contribution of the interfaces LEE measurements were made both for the pure glasses and for the bulklike wurtzite-like ZnO crystals.

Independently we measured the optical dielectric susceptibility of the film by the ellipsometric method using an ellipsometer with a spectral resolution up to 1.2 nm mm^{-1} within the 2.5–6.2 eV spectral range. The latter gives a possibility of determining the imaginary part

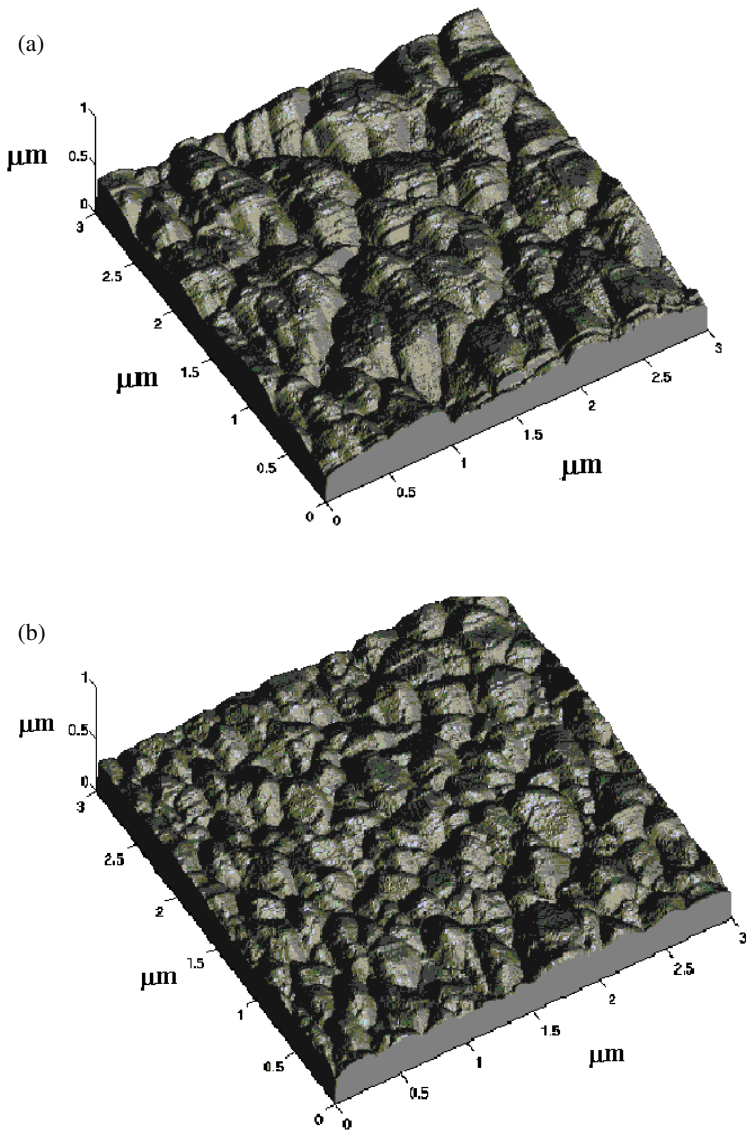

Figure 1. AFM three-dimensional images of the ZnO films prepared at different spraying flow rates with their mean grain size: (a) $f = 7.5$ ml min^{-1} with $\langle d_s \rangle = 0.66$ μm; (b) $f = 3.7$ ml min^{-1} with $\langle d_s \rangle = 0.45$ μm.

of the dielectric susceptibility ε_2 with accuracy better than 3.6%. To extract the influence of the bare glass substrate all the ellipsometric measurements were also made for the pure glass substrate.

3. Molecular dynamics interface optimization on the ZnO crystal–glass interfaces

Structural optimization of the ZnO film–glass interfaces plays a key role in understanding the origin of the observed effects and it was performed in two steps.

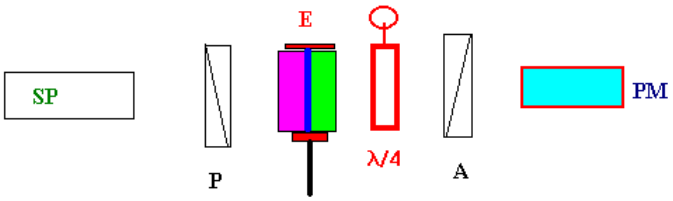

Figure 2. Principal set-up for the Senarmone measurements. The detailed explanations are given in the text.

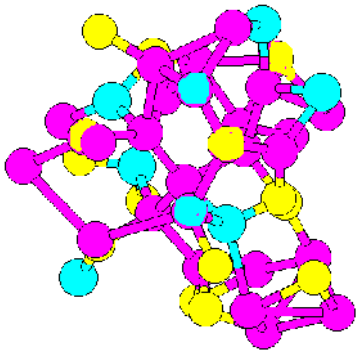

Figure 3. Topological structure of the bare glass–ZnO thin interface layers simulated using the MD method: oxygen—red; silicon—blue; Zn—yellow.

Initially we determined the energetically most favourable structure (corresponding to minimal total energy) using the MM+ self-consistent force field approach within the HyperChem 7.0 program [9]. The calculation technique is similar to the technique developed by us earlier for the glass [10]. MD was performed using a 6–31 G basis set [9] using a density functional theory (DFT) level (Lee–Yang–Parr correlation function) [11] together with Becke's gradient correlation [12].

The procedure was initiated for the fourth neighbouring layers (two from the film's crystallite side and two from the bare glass substrate) similarly as in [13]. About 80–100 atoms from both sides of the interface have been included. At the second step, the next proper layer was considered, and the procedure was repeated for the new value of total energy per ion. The iteration process was continued until the relative displacement of the ions for two successive layers was <0.14 Å.

During the second step (more precise approach) the initially optimized reconstructed surface (near-interface ZnO) sheets (obtained previously) were additionally treated using an *ab initio* Car–Parrinello MD scheme [14] within a DFT norm-conserving pseudopotential (NCPP) scheme. The functional used in the CPMD was of the Kleinman–Bylander type [15]. We used a PW cut-off of 37 Ryd. The computed bond lengths agreed with the experimental values up to 2%. The performed evaluations have shown that the LDA approach underestimates the ZnO bulk lattice constant by 1.54%, while the pseudopotential approximation overestimates it only by 0.18%. The preferable geometry corresponds to the lattice constants given by about $\boldsymbol{a} = 3.259$ Åand $\boldsymbol{c} = 5.2081$ Å.

The typical structure of the interface appearing on the border (thin layer about 1–1.5 nm) between the bare glass and the ZnO single crystallite is shown in figure 3. The role of this thin layer is crucial for the size-dependent behaviour of the ZnO crystallites (see table 2).

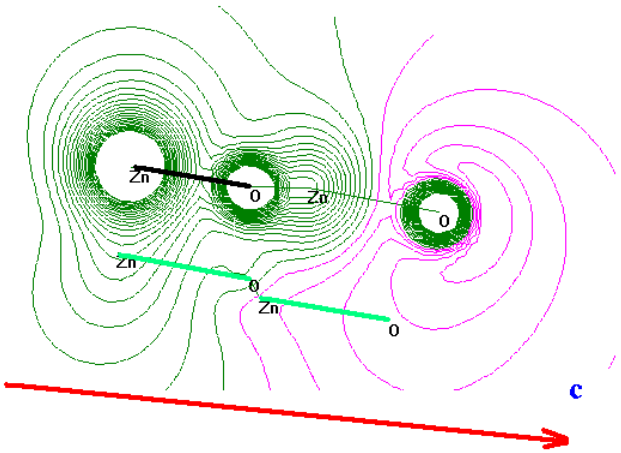

Figure 4. Distribution of the electrostatic potential for the 0.2 nm pure ZnO films near the bare glass interface before fluorine introduction. Axis $\boldsymbol{c}$ corresponds to the direction perpendicular to the interface.

Table 2. Changes of effective structural parameters of the ZnO single crystallites versus the distance $\boldsymbol{d}$ between the bare glass border and the ZnO films. In the brackets are given the same parameters for the F-doped ZnO.

Distance $\boldsymbol{d}$ from the glass–ZnO interface (nm)	$\boldsymbol{a}$ (nm), ZnO–6H (wurtzite structural component)	$\boldsymbol{c}$ (nm) (wurtzite structure)
0.2	2.889(4) (**2.872**)	5.515(2) (**5.523**)
0.4	2.16(3) (**2.912**)	5.486(1) (**5.493**)
0.6	2.937(1) (**2.935**)	5.450(6) (**5.458**)
0.8	2.956(5) (**2.955**)	5.412(4) (**5.416**)
1.0	2.974(4) (**2.973**)	5.378(2) (**5.381**)
1.2	3.002(2) (**3.002**)	5.267(3) (**5.268**)
1.4	3.112(4) (**3.112**)	5.134(9) (**5.134**)
1.6	3.251(1) (**3.251**)	5.209(3) (**5.209**)
1.8	3.258(6) (**3.257**)	5.2072(4) (**5.207**)
2.0	3.258(1) (**3.258**)	5.2071(0) (**5.207**)

One can see that the Zn–O chemical bonds (see table 2) are dependent on the Zn–O bond distance on moving from the ZnO–glass border towards deeper ZnO layers and the ratio $\boldsymbol{c/a}$ increases. An analogous increase is also observed for the ZnO–F films.

In figures 4–6 is presented the local charge density distribution versus the distance $\boldsymbol{d}$ obtained by the method described above. The Zn–O–Zn distances show additional charge density non-centrosymmetry on nearing the mentioned interface border and fluoridation. There are two main contributions to the charge density non-centrosymmetry. The first one is connected with the presence of the ZnO–glass interface. The second one is caused by involvement of the highly polarized fluorine ions, causing additional charge density polarization.

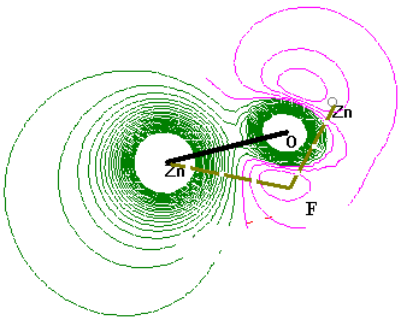

Figure 5. Changes of local charge density distribution after introducing F for the deep ZnO crystallites (larger than 2 μm).

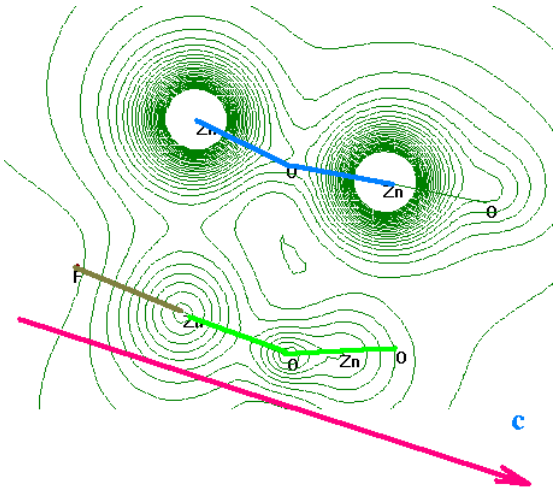

Figure 6. Disturbances of the local Zn–O distribution due to the influence of F for the distance about 0.2 nm from the surface.

4. Band structure features

4.1. Calculation method

Emerging from the structure of reconstructed ZnO single-crystalline surfaces (see table 2 and figures 3–6), one can expect the appearance of a substantially modified $E(\boldsymbol{k})$-dispersion.

There exist several works devoted to the BS calculations of the perfect bulk ZnO crystals (see for example [16]). For description of the optical properties we have chosen the NCPP scheme introduced in [17]. This method has just been successfully applied for description of the optical properties of different semiconductors and dielectrics [13], including glass [10].

During the calculations we have included 2s, 2pO, 3d, 4s Zn and 2s, 2p F occupied orbitals and 3s, 3p O, 4p Zn and 3s, 3p F excited orbitals. The technique of calculation of the secular equation's matrix elements is described in detail elsewhere (see for example [13]). A method of special points [18] was applied for numerical calculation of spatial electron charge density distribution. Eigenenergy convergence equal to about 0.02 eV was achieved using 320–490 PW functions.

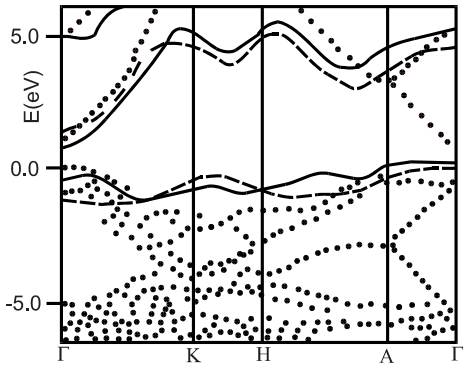

Figure 7. Band energy structure of the ZnO crystalline films doped by F on the glass substrate calculated by the NCPP method. By the solid curve are indicated the deviations connected with the influence of substrate and fluoridation for the film thickness 1 μm; by the dashed curve those for the film thickness 1.5 μm. The perfect BS is indicated by the dots.

The following condition was chosen as a criterion for satisfying self-consistency:

$$|(\rho_m - \rho_{m-1})/\rho_m| < \varepsilon, \tag{2}$$

where ρ_m is the charge density for the mth iteration; ε is adopted as 0.02.

For verification of the method we performed calculations of the BS for the ZnO perfect crystals and we have achieved a degree of coincidence (with [16]) better than 1.3%. Acceleration of the iteration convergence was achieved by transferring 83% of the $(m-1)$th iteration with respect to the mth iteration.

4.2. Results of the BS calculations

A typical fragment of the BS dispersion calculated for the ZnO wurtzite structure with and without fluorine doping including interface structural reconstruction is shown in figure 7 for film thickness 1 and 1.8 μm. One can see that the reconstructed surfaces favour substantial deviations in the BS $E(\boldsymbol{k})$ dispersion compared with the perfect ZnO crystals. Simultaneously one can observe a substantial energy shift of the effective top of the valence and conduction bands. Moreover BS dispersion is only slightly dependent on the film thickness.

For convenience we show only principal deviations for the top of the valence band and the bottom of the conduction band. The occurrence of the flatter band dispersion indicates the crucial role of the reconstructed surface states.

5. Dispersion of refractive indices and electro-optic coefficients

Before simulation of the LEE properties we performed calculations of the imaginary part of the linear optical susceptibility $\varepsilon_2(E)$ responsible for the linear optical effects. $\varepsilon_2(E)$ is directly connected with the inter-band optical transitions determining the corresponding BS of the reconstructed crystalline surfaces:

$$\varepsilon_2(E) \cong \frac{2\pi N m e^2 \hbar^2}{c^3} \sum_{\vec{k}j,l} |\vec{\mu}^2_{jk}| \delta(E_j(\vec{\vec{k}}) - E_l(\vec{\vec{k}}) - E) \tag{3}$$

where N is the density of the appropriate valence electron states; μ_{jl} are optical transition dipole moments between the jth and lth band states evaluated by numerical integration over the occupied band states at different $\boldsymbol{k}$-points of the BZ.

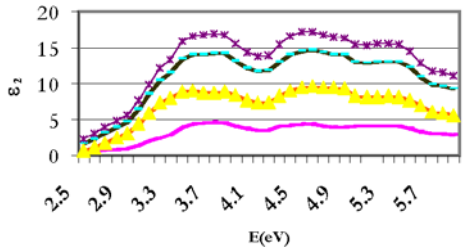

Figure 8. Spectral dependences of ε_2 for the pure ZnO films (– – –, theoretically calculated; ▲, experimentally measured) and ZnO–F(1%) films (- - - -, theoretically calculated; ★, experimentally measured).

The spectral dependences of $\varepsilon(E)$ calculated by the method described above are presented in figure 8. The spectrum of $\varepsilon_2(E)$ has three principal maxima both for the fluorine-doped (3.5–4.0, 4.6–4.8, 5.1–5.35 eV) and for the pure (3.8–4.0, 4.7–4.8, 5.2–5.35 eV) films. The calculations predict a slight spectral shift of the observed maxima (up to 0.2–0.3 eV). A dominant contribution to $\varepsilon_2(E)$ therefore belongs to the ZnO bulklike states. We predicted a drastic increase of ε_2 values (up to 2.8-fold). Such behaviour originates from the flattening of the BS dispersions and corresponding enhancement of the density of states (see figure 7). The experimental ellipsometric measurements confirm this prediction (see figure 8). Several discrepancies between theory and experimental data in the values of $\varepsilon_2(E)$ may be caused by morphological disturbances (see figure 1). It is necessary to add that neither the pure glass itself nor the ZnO wurtzite-like crystallites manifest such striking effects.

The LEE is described by the expression

$$\Delta n_{ij}^{(\omega)} = r_{ijk}(\omega, \omega, 0) E_k^{(0)} \tag{4}$$

where Δn_{ij} is the birefringence, E_k^0 is the electrostatic field strength and r_{ijk} is the LEE coefficient directly connected with the second-order non-linear optical susceptibility χ_{ijk}.

Emerging from general expressions connecting the macroscopic second-order non-linear optical susceptibility χ_{ijk} and microscopic hyperpolarizability β_{ijk}we can write

$$\chi_{ijk}^{(\omega,\omega,0)} = f_i^{(\omega)} f_j^{(\omega)} f_k^{(0)} \beta_{ijk}^{(\omega,\omega,0)}, \tag{5}$$

where $\chi_{ijk}^{(\omega,\omega,0)}$ is a macroscopic second-order nonlinear susceptibility responsible for the LEE; $f_{i,j,k}^{(\omega)}$ are the i, j, k components of the local Lorenz fields.

Using the oversimplified expression we can present the microscopic hyperpolarizability in the form

$$\beta_{ijk}^{(\omega,0)} \simeq \frac{\vec{\mu}_{gr}^2 \Delta\vec{\mu}_{tr}(j \to l)}{|E_j - E_l|^3} \tag{6}$$

where μ_{gr} is a ground-state dipole moment and $\Delta\mu_{gr}(j \to l)$ the transition dipole moments between j and l band states described by equation (5).

From a comparison between equations (2)–(5) and (6) one can see that the observed increase of $\varepsilon_2(E)$ values should also favour an increase of the $\chi_{ijk}^{(\omega,\omega,0)}$ directly connected with the r_{ijk}. The data calculated by a method described above are presented in table 3.

From table 3 one can see a substantial difference in the values of the r_{ijk} tensor component distribution. The calculated data also allow us to estimate changes of refractive indices (using Kramers–Kronig analysis) (see figure 9). Doping by fluorine favours increasing refractive indices.

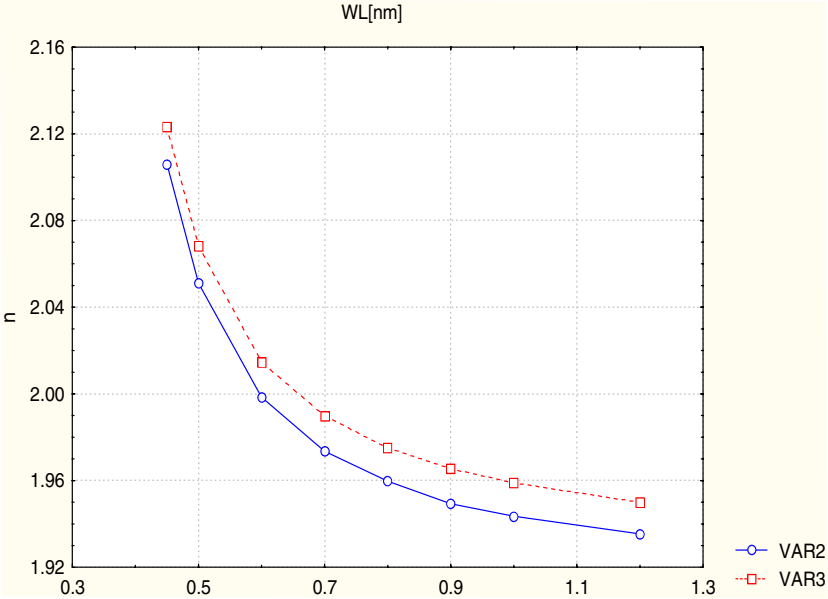

Figure 9. Dispersion of ordinary refractive indices for pure (○) and fluorine-doped ZnO (□) films.

Table 3. Evaluated values of the Pockels r_{ijk} tensor components at different wavelengths.

λ (nm)	r_{222} (pm V^{-1})	r_{212} (pm V^{-1})
750	4.81	2.18
700	4.89	2.31
650	5.01	2.52
550	6.01	2.84
500	7.56	3.01
450	10.6	3.86
400	15.2	4.01

The observed LEE values increase correlating with $\varepsilon_2(E)$ and refractive index n (compare table 3 and figure 10). The effects are stronger for the fluorine-doped materials. This fact confirms a crucial role of the glass–film substrates as well of the doping by fluorine in the observed behaviours.

The spectral measurements of electro-optics coefficients (see figure 10) confirm theoretical predictions (table 3). For the wavelengths shorter than 420 nm the increase of the r_{222} coefficient reaches a value of about 17 pm V^{-1}. Such a giant increase of the Pockels coefficient in a blue spectral range may open a new step in the design of compact thinlike electro-optic light modulators for blue lasers.

6. Conclusions

We have theoretically predicted and experimentally proved a large increase (up to one order) of the linear electro-optics of ZnO wurtzite-like films doped by fluorine and deposited on bare glasses. Using the NCPP BS calculations as well as MD interface structural optimization we have predicted that due to addition of fluorine one can expect a substantial increase of the

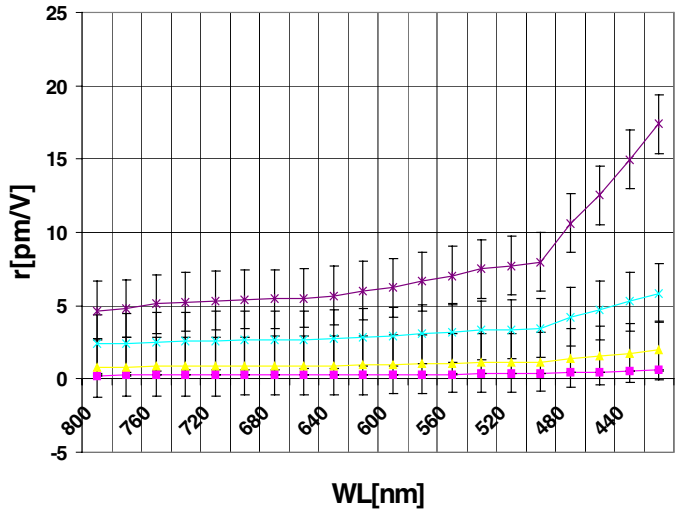

Figure 10. Spectral dependences of r_{222} for different ZnO specimens: ■, pure ZnO crystals; ■, ZnO films deposited on bare glass substrate; × - - - -, r_{212} tensor component for the ZnO–bare glass interface; × - - - -, r_{222} for the ZnO–F–bare glass interface.

charge density non-centrosymmetry on the interface separating the bare glass substrate and the appropriate film, the imaginary part of the optical dielectric susceptibility, the refractive indices and the Pockels coefficients. A good agreement between the obtained experimental results and predicted theory is achieved. A possibility of simultaneous use of interface charge density non-centrosymmetry together with the appropriate doping to enhance the LEE tensor coefficients is demonstrated.

The discovered phenomenon opens a promising way for design of competitive miniaturized electro-optics devices in the blue spectral range.

References

[1] Chaillaud F, Smith A and Baumard J F 1993 *J. Am. Ceram. Soc.* **76** 998
[2] Chen Q, Qian Y, Chen Z, Zhou G and Zhang Y 1995 *Mater. Lett.* **22** 93
[3] Chen M, Pei Z L, Sun C, Wen L S and Wang X 2000 *J. Cryst. Growth* **220** 254
[4] Sanchez-Juares A, Tiburcio-Silver A and Ortiz A 1998 *Sol. Energy Mater. Sol. Cells* **52** 301
[5] Nakanishi Y, Miyake A, Kominami H, Aoki T, Hatanaka Y and Shimaoka G 1999 *Appl. Surf. Sci.* **142** 233
[6] Ahmin A 1989 *J Am. Ceram. Soc.* **72** 369
[7] Kityk I V, Ebothe J and Elchichou A 2001 *Nonlinear Opt.* **21** 121
[8] Mirtwa R and Gunter P 1982 *Theory of the Electrooptics Measurements* (New York: Kluwer)
[9] HyperChem 7.0 2002 webpage http://www.hypercube.com
[10] Kityk I V and Sahraoui B 1999 *Phys. Rev.* B **60** 942
[11] Lee C, Yang W and Parr C G 1998 *Phys. Rev.* B **37** 785
[12] Becke A D 1988 *Phys. Rev.* A **38** 3098
[13] Kityk I V, Kasperczyk J and Andrievskii B V 1996 *Phys. Lett.* A **216** 161
Kityk I V, Smok P, Berdowski J, Lukasierwicz T and Majchrowski A 2001 *Phys. Lett.* A **280** 70
[14] Car R and Parinello M 1990 *Phys. Rev.* B **42** 7470
[15] Bylander B M and Kleinman L 1990 *Phys. Rev.* B **41** 7868
[16] Hill N A and Waghmare U 2000 *Phys. Rev.* B **62** 8802
[17] Bachelet G B, Hamann D R and Schluter M 1982 *Phys. Rev.* B **26** 4199
[18] Chadi D J and Cohen M L 1973 *Phys. Rev.* B 8 5747
[19] Addou M, Moumin A, El Idrissi B, Regraui M, Bougrine A and Kachouane A 1999 *J. Chem. Phys.* **96** 232